# Information Flow and Cooperative Control of Vehicle Formations

J. Alexander Fax * Richard M. Murray †

15 April 2003
Submitted, *IEEE T. Automatic Control*

**Abstract**

We consider the problem of cooperation among a collection of vehicles performing a shared task using intervehicle communication to coordinate their actions. We apply tools from graph theory to relate the topology of the communication network to formation stability. We prove a Nyquist criterion that uses the eigenvalues of the graph Laplacian matrix to determine the effect of the graph on formation stability. We also propose a method for decentralized information exchange between vehicles. This approach realizes a dynamical system that supplies each vehicle with a common reference to be used for cooperative motion. We prove a separation principle that states that formation stability is achieved if the information flow is stable for the given graph and if the local controller stabilizes the vehicle. The information flow can be rendered highly robust to changes in the graph, thus enabling tight formation control despite limitations in intervehicle communication capability.

## 1 Introduction

Recent technological advances have spurred a broad interest in autonomous, adaptable vehicle formations. The development of powerful control techniques for single vehicles, the explosion in computation and communication capabilities, and the advent of miniaturization technologies have elevated interest in vehicles which can interact autonomously with the environment and other vehicles to perform, in the presence of uncertainty and adversity, tasks beyond the ability of individual vehicles. Application areas include microsatellite clusters [4, 27, 34], unmanned aerial vehicles (UAVs) [5, 18, 32], autonomous underwater vehicles (AUVs) [8, 29], and automated highway systems (AHS) [1, 28, 30].

*Corresponding Author. Address: Northrop Grumman Corp., 21240 Burbank Blvd, Woodland Hills, CA 91367. Tel. 818-715-5101. Alex.Fax@ngc.com. Research supported by AFOSR grants F49620-99-1-0190 and F49620-01-1-0460. First author also supported by an NSF Graduate Research Fellowship and an ARCS Foundation Fellowship.

†Address: Control and Dynamical Systems, California Institute of Technology. Pasadena, CA 91125. Tel. 626-395-6460. murray@cds.caltech.edu.

While each of these areas poses its own unique challenges, several common threads can be found. In most cases, the vehicles are coupled through the task they are trying to accomplish, but are otherwise dynamically decoupled, meaning the motion of one does not directly affect the others. Decisions must be made by each vehicle using only limited information, about the other vehicles, information that may be subject to uncertainty and transmission delay. The reaction of a vehicle to other vehicles' motions renders the formation an interconnected dynamical system whose behavior depends not only on the individual vehicle dynamics, but on the nature of their interconnection.

Existing approaches to vehicle formation control generally fall into two cagetories. The first is the "leader-follower" approach. This approach as the advantage of simplicity in that a reference trajectory is clearly defined by the leader, and that stability of the formation is implied by stablity of the individual vehicles' control laws. Leader-follower architectures are known to have poor disturbance rejection properties (see, e.g., [33]). Additionally, a leader-follower architecture depends heavily on the leader for achieving its goal, and over-reliance on a single vehicle in the formation may be undesirable, especially in adversarial environments. The second approach is the "virtual leader" approach [12, 22, 29], in which vehicles in the formation jointly synthesize a single fictitious leader vehicle whose trajectory acts as a leader for the group. This approach avoids the problems with disturbance rejection inherent in the leader-follower approach, but at the expense of high communication and computation capabities needed to synthesize the virtual leader and communicate its position.

What these approaches have in common is an assumption about the underlying communication topology that enables the use of a particular formation control methodology. We wish to consider a broader range of vehicle interconnection possibilities and understand how the topology of the information flow affects the stability and performance of the system as it performs a coordinated task. Our ultimate goal is the development of information exchange strategies which improve formation stability and performance and are robust to changes in the communication topology.

Our approach is to model the communication topologies as a graph; each vehicle is a node of a (directed) graph, and an arc is drawn from node $i$ to node $j$ if vehicle $i$ receives information from vehicle $j$. By merging ideas from graph theory, control theory, and dynamical systems theory, we are able to study the interplay between the communication network and vehicle dynamics, and to propose strategies for information exchange which mitigate those effects. We limit our focus to LTI systems in order to elucidate the role of the graph in the system behavior. In that context, we provide necessary and sufficient conditions for stability of an interconnected system of indentical vehicles in terms of the eigenvalues of the graph Laplacian and show how to shape the information flow to achieve high performance. Portions of this work have been reported in [13, 14, 15].

The paper is organized as follows. We begin with a motivating example in the next section that establishes some of the key concepts that we wish to explore. In Section 3 we provide a brief

summary of the relevant results in graph theory and define the relevant notation. The main stability results are derived in Section 4, where we give a Nyquist-like criteria for determining stability and explore the interaction between graph topology and vehicle dynamics through this criteria. In Section 5, we propose an information exchange methodology which is robust to uncertainty in the communication topology. This approach exhibits a separation principle which decouples the stability of the formation communication, which we term information flow, and the local control of individual vehicles. Finally, in Section 6 we summarize the main results and provide some thoughts on future directions of research.

## 2 Motivating Example

To better illustrate the class of systems that we are interested in exploring, we consider the system illustrated in Figure 1(a). The system consists of 6 identical vehicles. Each vehicle is able to sense some collection of other vehicles and transmit information to some separate set of vehicles. The goal is for the vehicles to form a regular hexagon, with each vehicle maintaining the proper position relative to its neighbors. The initial conditions of the vehicles is shown in Figure 1(a), along with lines indicating which vehicles can see one another in this example.

To make the example more concrete, we model the vehicles as double integrators with a communication time delay. The dynamics in the $x$ and $y$ axes are then given by $P(s) = \frac{e^{-sT}}{s^2}$. We choose a simple PD controller for each axis, of the form $K(s) = K_p + K_d s$, with the input to the controller given as the average error between the actual and desired positions with respect to the vehicle's "neighbors." Initially we will choose these neighbors to be the vehicles that are to the left and right of the given vehicle in its final configuration. Note that because the dynamics in each axis are decoupled, we can consider each axis independently and hence it is sufficient to analyze the stability of a single axis.

The full system dynamics consist of the individual vehicle dynamics interconnected by the "sensed" information flow corresponding to computing the average error with respect to the left and right neighbors. The plant and controller dynamics are decoupled, but the error vector

The error vector is given by

$$u = L(y - y_d) \qquad L = \begin{bmatrix} 1 & -\frac{1}{2} & 0 & 0 & 0 & -\frac{1}{2} \\ -\frac{1}{2} & 1 & -\frac{1}{2} & 0 & 0 & 0 \\ 0 & -\frac{1}{2} & 1 & -\frac{1}{2} & 0 & 0 \\ 0 & 0 & -\frac{1}{2} & 1 & -\frac{1}{2} & 0 \\ 0 & 0 & 0 & -\frac{1}{2} & 1 & -\frac{1}{2} \\ -\frac{1}{2} & 0 & 0 & 0 & -\frac{1}{2} & 1 \end{bmatrix}, \tag{1}$$

where $L$ is the matrix that defines the toplogy of the sensed information for each of the two (decoupled) axes.

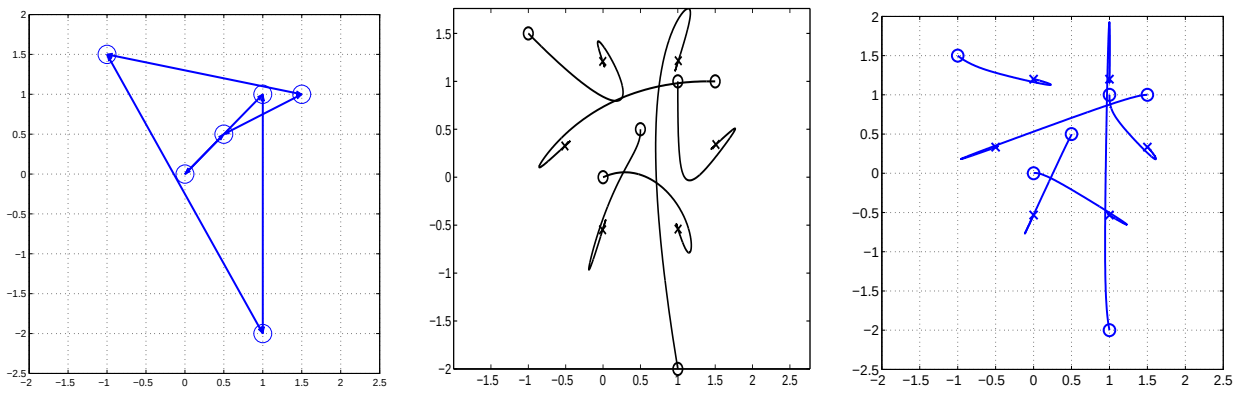

Figure 1: Hexagon stabilization: (a) initial condition and sensing topology, (b) sensed information only, (c) sensed and communicated information flow.

The stability of the system is easily determined by computing the stability of the fully interconnected system. However, this straightforward calculation gives us little insight into how the choice of the set of neighbors affects the closed loop performance. What if, for example, we had chosen to have each vehicle look at its two nearest neighbors and the vehicle across from it in the formation? Would it still be stable? We provide an answer to this question in Section 4, where we show that the eigenvalues of $L$ can be used as part of a Nyquist criterion to determine stability of the interconnected system.

As the condition that we derive shows, it is possible for the vehicles to be formally stable, but to exhibit very poor performance. This is illustrated in Figure 1(b). The poor performance of the controller is due to the fact that the initial positions of the vehicles are far from their final values. However, each vehicle is simply trying to position itself relative to its final set of neighbors and hence it may move in the completely wrong direction initially.

A final set of questions relates to the design of the information flow to reach a shared consensus about the control objective. In particular, in the formulation above, we have only used sensed information to stability the formation. What if we could also transmit information to a potentially different set of vehicles? As an example, suppose that the vehicles were to first reach consensus about the desired center of the overall formation and then were regulate their position relative to that center. This could give much better results than simply looking at one's neighbors since spurious transients due to each vehicle trying to react to motion of its neighbors could be eliminated. Indeed, as shown in Figure 1(c), appropriate use of transmitted information can significantly reduce the spurious transients, while still providing feedback to insure robustness of the overall formation. It is important to note that this consensus is still performed in a distributed fashion: no single vehicle is designated as a "leader," the topology of the graph is not known to any vehicle, nor is any centralized computation performed to determine the center of the position.

# 3 Graph Theory

Many excellent texts on graph theory exist; a recent example is by Diestel [11]. Recent results regarding the Laplacian and its spectral structure can be found in the work of Merris [23, 24] and Chung [6]. Perron-Frobenius theory can be found in many texts; the presentation here is based on material in [2, 20, 31].

We now introduce some notation which we will use in the remainder of the thesis. Variables in lower case refer to scalars, vectors or elements of sets; the distinction will be clear from context. Variables in upper case refer to matrices, and calligraphed letters refer to sets or graphs. When $v$ is a vector, $v_i$ refers to the $i$th element of that vector, and when $v$ is a set, $v_i$ refers to the $i$th indexed element of that set. $|\mathcal{G}|$ denotes the cardinality of the set $\mathcal{G}$. $A_{ij}$ refers to the element occupying the $i$th row and $j$th column of $A$. $I_n$ refers to the $n \times n$ identity matrix.

## 3.1 Basic Definitions

A *directed graph* $\mathcal{G}$ consists of a set of vertices, or nodes, denoted $\mathcal{V}$, and a set of arcs $\mathcal{A} \subset \mathcal{V}^2$, where $a = (v, w) \in \mathcal{A}$ and $v, w \in \mathcal{V}$. The first element of $a$ is denoted tail$(a)$, and the second is denoted the head$(a)$. It is said that $a$ points from $v$ to $w$. We will assume that tail$(a) \neq$ head$(a)$ for all $a$, meaning that the graph has no self-loops. We also assume that each element of $\mathcal{A}$ is unique. A graph with the property that for any $(v, w) \in \mathcal{A}$, the arc $(w, v) \in \mathcal{A}$ as well is said to be *undirected*; in undirected graphs the pair of arcs is often modeled as a single edge with no direction associated to it. The *in(out)-degree* of a vertex $v$ is the number of arcs with $v$ as its head (tail). If every possible arc exists, the graph is said to be *complete*.

A *path* on $\mathcal{G}$ of length $N$ from $v_0$ to $v_N$ is an ordered set of distinct vertices $\{v_0, v_i, \ldots, v_N\}$ such that $(v_{i-1}, v_i) \in \mathcal{A}$ for all $i \in [1, N]$. An *$N$-cycle* on $\mathcal{G}$ is defined the same as a path except that $v_0 = v_N$, meaning the path rejoins itself. A graph without cycles is said to be *acyclic*. A graph with the property that the set of all cycle lengths has a common divisor $k > 1$ is said to be *$k$-periodic*.

If a path exists from $v_i$ to $v_j$, it is said that $v_i$ has *access* to $v_j$. A graph with the property that every vertex has access to every other vertex is said to be *strongly connected*. (A graph consisting of a single vertex with no arcs is also considered strongly connected.) A graph in which disjoint subsets of vertices exists whose elements do not have access to one another is termed *disconnected*. Note an undirected graph is either strongly connected or disconnected.

## 3.2 Algebraic Graph Theory

One area of graph theory which will be of significant interest to us is algebraic graph theory, which studies relationships between the structure of graphs and different matrix representations

of graphs. For the purpose of defining graphs, we assume that the vertices of $\mathcal{G}$ are enumerated, and each is denoted $v_i$. The *adjacency matrix* of a graph, denoted $A(\mathcal{G})$, is a square matrix of size $|\mathcal{V}|$, defined by $A_{ij} = 1$ if $(v_i, v_j) \in \mathcal{A}$, and is zero otherwise. When the graph in question is clear, the adjacency matrix will be denoted as $A$. Note that $A$ uniquely specifies a graph, although $A$ itself is not unique for a given graph, as it depends on the enumeration of the vertices. However, two adjacency matrices of the same graph are necessarily similar to one another via a permutation matrix. As such, it is clear that the eigenvalues of $A$ are uniquely specified by the graph (though the converse is not true), and early research in algebraic graph theory focused on the relationship between eigenvalues of $A(\mathcal{G})$ and graph-theoretic properties of $\mathcal{G}$ [9, 10].

Our work will make use of a different graph which has been the object of study more recently. Let $D$ be the matrix with the out-degree of each vertex along the diagonal. The *Laplacian* of the graph is defined as[1]

$$L = D^{-1}(D - A). \tag{2}$$

In the event that $D$ is singular due to a vertex $v_i$ with zero out-degree, set $D_{ii}^{-1} = 0$ to complete the definition. Note that $L$ of Equation 1 corresponds to the graph in Figure 1. We will further denote the weighted adjacency matrix $I - L$ as $G$.

$L$ can be viewed as a normalized version of the adjacency matrix. In this construction, each arc leading into a given vertex is weighted equally such that the weights sum to one. More generally, it is possible to work with weighted graphs, in which the off-diagonal elements of $L$ are unequal yet still sum to $-1$. Most of the results of the following sections do not depend on the arcs being weighted equally, though we will assume that for convenience.

A property of the Laplacian is that $G$ is nonnegative by construction. The theory of nonnegative matrices, much of which derives from the celebrated Perron-Frobenius theorem, will be quite useful in understanding the links between graph theory and vehicle formation control. The results of this section can be found in [2, 20, 31].

A matrix $A$ is *positive (nonnegative)* if each element is positive (nonnegative). Given two nonnegative $n \times n$ matrices $A, B$, we say $A > B$ ($A \geq B$) if $A - B$ is positive (nonnegative). A square nonnegative matrix $A$ is *reducible* if there exists a permutation matrix $P$ such that $PAP^T$ can be represented

$$PAP^T = \begin{pmatrix} A_{11} & 0 \\ A_{21} & A_{22} \end{pmatrix}, \tag{3}$$

where $A_{11}, A_{22}$ are square, or if $n$=1 and $A = 0$. A matrix which is not reducible is said to be *irreducible*. As will be clear later, reducibility of a Laplacian corresponds to the presence of leaders

[1]Some references define $L$ as $D - A$. Others use the transpose of $A$ to define the Laplacian of the directed graph. This distinction is of little consequence in terms of the theory, but the definition stated above better suits our purposes.

in the formation structure. As such, the properties of reducible matrices are useful in understanding the workings of leader-follower architectures. Because the goal of this paper is to explore formations which do not exhibit leader-follower structures, we will forego a detailed discussion of reducible matrices and their role in formation analysis. The interested reader can explore this topic in [13].

Just as in Section 3.2 a directed graph was used to define a matrix, a square matrix can also be used to define a directed graph. This graph, denoted $\mathcal{G}(A)$, has $n$ vertices denoted $v_1, \ldots, v_n$, and $(v_i, v_j) \in \mathcal{A}$ if $A_{ij} \neq 0$. Unlike the directed graphs discussed above, $\mathcal{G}(A)$ may contain loops if $A_{ii} \neq 0$. It should be clear that the directed graph associated with $A(\mathcal{G})$ is in fact $\mathcal{G}$ itself.

The following theorem relates a nonnegative matrix with its directed graph, as well as supplying an algebraic characterization:

**Theorem 1.** *Given a nonnegative $n \times n$ matrix $A$, the following are equivalent:*

1. *$A$ is irreducible.*
2. *$A^T$ is irreducible.*
3. *$\mathcal{G}(A)$ is strongly connected.*
4. *$(I_n + A)^{n-1} > 0$.*

If $\mathcal{G}(A)$ is aperiodic, then $A$ is termed *primitive*. If $\mathcal{G}(A)$ is $k$-periodic, it is termed imprimitive, or *cyclic of index $k$*.

The following celebrated theorem was proven for positive matrices by Perron and extended to irreducible matrices by Frobenius. We will denote the spectral radius of a matrix $A$ as $\rho(A)$.

**Theorem 2 (Perron-Frobenius).** *Let $A$ be a nonnegative, irreducible matrix. The following are true:*

1. *$\rho(A) > 0$.*
2. *$\rho(A)$ is a simple eigenvalue of $A$, and any eigenvalue of $A$ of the same modulus is also simple.*
3. *$A$ has a positive eigenvector $x$ corresponding to $\rho(A)$.*
4. *$B > A \Rightarrow \rho(B) > \rho(A)$.*

*Furthermore, if $A$ is primitive, then all eigenvalues of $A$ other than $\rho(A)$ have modulus strictly less than $\rho(A)$.*

If $A$ is not primitive, the eigenvalues of $A$ have an interesting structure:

**Theorem 3.** *Let $A$ be a nonnegative, irreducible matrix which is cyclic of index $k$. Then $A$ has $k$ eigenvalues of modulus $\rho(A)$, equal to*

$$\lambda_i = \rho(A) e^{\frac{2\pi j}{k} i}, \quad i = 0, \ldots, k-1. \tag{4}$$

### 3.3 Eigenvalues of Laplacians

We now return to the structure of the spectrum of the Laplacian. We begin with the observation that the rows of $L$ sum to zero by definition, which implies that

**Proposition 1.** *Zero is an eigenvalue of $L$.*

Furthermore, this condition implies that $1^T$ is the eigenvector associated with this eigenvalue. Of course, any eigenvalue $\lambda$ of $L$ corresponds to an eigenvalue $1-\lambda$ of $G$. Thus, $G$ has an eigenvalue of 1. The fact that this eigenvalue has a positive eigenvector implies that it is, in fact, the Perron root of $G$. We therefore conclude from the Perron-Frobenius theorem that

**Proposition 2.** *All eigenvalues of $L$ lie in a disk of radius 1 centered at the point $1+0j$ in the complex plane.*

We denote this region the *Perron disk*. We can apply further ideas from Perron-Frobenius theory:

**Proposition 3.** *If $\mathcal{G}$ is strongly connected, the zero eigenvalue of $L$ is simple. If, in addition, $\mathcal{G}$ is aperiodic, all nonzero eigenvalues lie in the interior of the Perron disk. If $\mathcal{G}$ is $k$-periodic, $L$ has $k$ evenly spaced eigenvalues on the boundary of the Perron disk.*

If $\mathcal{G}$ is undirected, then $L$ is similar to $I - D^{1/2}AD^{1/2}$, which is clearly symmetric, from which we conclude that

**Proposition 4.** *If $\mathcal{G}$ is undirected, then all eigenvalues of $L$ are real.*

If $\mathcal{G}$ consists of two disconnected components, it is clear that the multiplicity of the zero eigenvalue of $L$ is two. If, instead, the two components are connected by a small number of arcs, it follows from a perturbation argument that $L$ will have an eigenvalue near zero. For this reason, Fiedler [16] termed this eigenvalue the *algebraic connectivity* of the graph, and began a program of research which continues to this day relating this parameter to graph-theoretic concepts, including measures of connectivity in graphs.

## 4 Relative Position Control in Vehicle Formations

The problem we consider in this section is the stabilization of the relative position of a set of vehicles with identical linear dynamics.

### 4.1 Formation Equations of Motion

We consider a set of $N$ vehicles, whose (identical) linear dynamics are denoted

$$\dot{x}_i = P_A x_i + P_B u_i, \tag{5}$$

where $i \in [1, N]$ is the index for the vehicles in the flock. Note that each vehicle's dynamics are decoupled from the other vehicles. Each vehicle's sensed information is defined as follows:

$$y_i = P_{C_1} x_i \tag{6}$$

$$z_{ij} = P_{C_2}(x_i - x_j),\ j \in \mathcal{J}_i, \tag{7}$$

where the set $\mathcal{J}_i \subset [1, N]\backslash\{i\}$ represents the set of vehicles which vehicle $i$ can sense. Thus, $y_i$ represents internal state measurements, and $z_{ij}$ represents external state measurements relative to other vehicles. To obtain relative state measurements, a vehicle must have access, in this case via some form of sensing, to other vehicles' states. We assume that $\mathcal{J}_i \neq \emptyset$, meaning each vehicle can see at least one other vehicle. Note that a single vehicle cannot drive all the $z_{ij}$ terms to zero simultaneously; the errors must be synthesized into a single signal. For simplicity, we assume that all relative state measurements are weighted equally to form one error measurement:

$$z_i = \frac{1}{|\mathcal{J}_i|} \sum_{j \in \mathcal{J}_i} z_{ij}. \tag{8}$$

The choice of weighting does not impact the results of this section, as long as the weights for a given vehicle sum to one. We also define a decentralized control law $K(s)$ which maps $y_i, z_i$ to $u_i$, represented in state-space form by

$$\begin{aligned} \dot{v}_i &= K_A v_i + K_{B_1} y_i + K_{B_2} z_i \\ u_i &= K_C v_i + K_{D_1} y_i + K_{D_2} z_i. \end{aligned} \tag{9}$$

We now consider the system of all $N$ vehicles together. When the $i$ subscript is omitted, the vector is comprised of all $N$ vehicles' variables. Using this notation, the system dynamics are represented as follows:

$$\begin{pmatrix} \dot{x} \\ \dot{v} \end{pmatrix} = \begin{pmatrix} \widehat{P}_A + \widehat{P}_B \widehat{K}_{D_1} \widehat{P}_{C_1} + \widehat{P}_B \widehat{K}_{D_2} \widehat{P}_{C_2} L_{(n)} & \widehat{P}_B \widehat{K}_C \\ \widehat{K}_{B_1} \widehat{P}_{C_1} + \widehat{K}_{B_2} \widehat{P}_{C_2} L_{(n)} & \widehat{K}_A \end{pmatrix} \begin{pmatrix} x \\ v \end{pmatrix}, \tag{10}$$

where $\widehat{A} = I_N \otimes A$, $\otimes$ representing the Kronecker product, indicates the matrix $A$ repeated $N$ times along the diagonal. The resulting system is block diagonal with the exception of the matrix $L_{(n)}$, which contains the relative sensing information of Equation (8). $L$ is defined as follows:

$$L_{ii} = 1 \tag{11}$$

$$L_{ij} = \begin{cases} -\frac{1}{|\mathcal{J}_i|}, & j \in \mathcal{J}_i \\ 0, & j \notin \mathcal{J}_i. \end{cases} \tag{12}$$

Of course, $L$ is the Laplacian of a graph to be defined in the next section. Letting $n$ be the dimension of $x_i$, $L_{(n)}$ is of dimension $Nn \times Nn$ and is defined by replacing each element of $L$ with that element multiplied by $I_n$ (i.e., $L_{(n)} = L \otimes I_n$), thus generating a version of $L$ dimensionally compatible with $x_i$.

The goal of the controller as defined above is to drive the states (or at least a subset of them) to a common value. In this problem definition, we are not concerned about the final value so long as the vehicles share it. For some applications, such as orienting underwater vehicles, this is an understandable goal. For other applications, such as relative satellite positioning, it is necessary to add an offset term to $z_{ij}$ to achieve the desired intervehicle spacing. We define a time-varying offset function $h : [1, N] \times [1, N] \times \mathbb{R} \to \mathbb{R}^m, i, j, t \mapsto h_{ij}(t)$ , where $m$ is the dimension of $z_{ij}$, which defines the intervehicle spacing. We assume that $h$ is defined so that for all $i, j, k$, $h_{ij} + h_{jk} = h_{ik}$. This definition means that it is possible to position each vehicle such that $z_{ij} = h_{ij}$ for all $i, j$. One way to generate such a function is to define an offset $h_{i0}(t)$ for each vehicle relative to an arbitrary reference. Letting $h_0(t)$ be the vector of $h_{i0}(t)$ offsets, the error signal is then defined by

$$z(t) = L_{(m)}(y(t) - h_0(t)). \tag{13}$$

The offset function acts as an input to the dynamical system. We assume that $h_{ij}(t)$ is bounded. Because BIBO stability is implied by internal stability for LTI systems, the actual value of the $h_{ij}$ terms does not play a role in the stability analysis, and will henceforth be omitted. In general, $h_{ij}$ will be chosen to be consistent with the open-loop dynamics of the vehicles in formation. We will not consider the case where $h$ is also a function of the measurements, which is the case for variable spacing policies discussed in [30, 33].

We are now able to identify the role of the sensing graph in the formation dynamics. The vehicles and their sensing indices $\mathcal{J}_i$ together form a graph, where each node represents a vehicle and an arc leads from node $j$ to node $i$ if $j \in \mathcal{J}_i$. Our assumption that each vehicle can sense at least one other vehicle implies that the out-degree of each vertex is at least 1. The matrix $L$ defined in Equation (11) is none other than the Laplacian of the graph, defined in Section 3.2. The normalization of the Laplacian is equivalent in our setting to our averaging of the $z_{ij}$ terms so no gain is added to the observed input. This stands in distinction to other examples in the literature which use the Laplacian-like matrices in analyzing stability of interconnected systems [26].

### 4.2 Formation Stability

We now consider the relationship between graph Laplacians and formation stability. We show the following to be true:

**Theorem 4.** *A local controller $K(s)$ stabilizes the formation dynamics in Equation (10) iff it*

*simultaneously stabilizes the set of $N$ systems*

$$\begin{aligned} \dot{x} &= P_A x + P_B u \\ y &= P_{C_1} x \\ z &= \lambda_i P_{C_2} x \end{aligned} \tag{14}$$

*where $\lambda_i$ are the eigenvalues of $L$.*

*Proof.* We will show the above to be true by transforming the closed-loop dynamics in the following way: Let $T$ be a Schur transformation of $L$, meaning the unitary matrix such that $U = T^{-1}LT$ is upper triangular with the eigenvalues of $L$ along the diagonal [20]. Clearly, $T_{(n)}$ is a Schur transformation of $L_{(n)}$. This transformation has the following useful property, a clear consequence of the block structure of the relevant matrices:

**Lemma 5.** *Let $X$ be an $r \times s$ matrix, and $Y$ be an $N \times N$ matrix. Then*

$$\hat{X} Y_{(s)} = Y_{(r)} \hat{X}. \tag{15}$$

*Proof.* Using Kronecker product algebra, both sides can be shown to be equal to $Y \otimes X$. ■

Applying this property to the system dynamics, we see if we let $\tilde{x} = T_{(n)}x$, and $\tilde{v} = T_{(m)}v$, we can rewrite Equation (10) as

$$\begin{pmatrix} \dot{\tilde{x}} \\ \dot{\tilde{v}} \end{pmatrix} = \begin{pmatrix} \widehat{P}_A + \widehat{P}_B \widehat{K}_{D_1} \widehat{P}_{C_1} + \widehat{P}_B \widehat{K}_{D_2} \widehat{P}_{C_2} U_{(n)} & \widehat{P}_B \widehat{K}_C \\ \widehat{K}_{B_1} \widehat{P}_{C_1} + \widehat{K}_{B_2} \widehat{P}_{C_2} U_{(n)} & \widehat{K}_A \end{pmatrix} \begin{pmatrix} \tilde{x} \\ \tilde{v} \end{pmatrix}. \tag{16}$$

The elements of the transformed system matrix are either diagonal or upper triangular. This means that stability of this system is equivalent to the stability of the systems along the diagonal, i.e.:

$$\begin{aligned} \dot{\tilde{x}}_i &= (P_A + P_B K_{D_1} P_{C_1} + \lambda_i P_B K_{D_2} P_{C_2}) \tilde{x}_i + P_B K_C \tilde{v}_i \\ \dot{\tilde{v}}_i &= (K_{B_1} P_{C_1} + \lambda_i K_{B_2} P_{C_2}) \tilde{x} + K_A \tilde{v} \end{aligned} \tag{17}$$

which is equivalent to the controller $K(s)$ stabilizing the system

$$\begin{aligned} \dot{x} &= P_A x + P_B u \\ y &= P_{C_1} x \\ z &= \lambda_i P_{C_2} x. \end{aligned}$$

■

We thus identify the Laplacian eigenvalues as the object of interest in understanding formation stability. In this context, the zero eigenvalue of $L$ can be interpreted as the unobservability of absolute motion of the formation in the measurements $z_i$. It seems that a prudent controller design

strategy is to close an inner loop around $y_i$ such that the internal vehicle dynamics are stable, and then to close an outer loop around $z_i$ which achieves desired formation performance. For the remainder of this paper, we concern ourselves solely with the outer loop. Hence, we assume from now on that $P_{C_1}$ is empty and that $P_A$ has no eigenvalue in the open right half plane. We do not wish to exclude eigenvalues along the $j\omega$ axis because many vehicle formations (e.g., vehicle platoons, satellite clusters) possess those, and the presence of unobservable secular or periodic motion of the formation may be tolerable in those cases. If $K(s)$ stabilizes the system in Equation (18) for all $\lambda_i$ other than the zero eigenvalue, we say that it stabilizes the *relative formation dynamics*.

Note that for a strongly connected graph or for a formation with a single leader, it can be shown that the only equilibrium point is in fact the desired relative position of the vehicles. Additionally, the theorem is equally applicable when the inputs are driven not to zero, but to some internally consistent set of offsets [13].

For SISO systems, we can state a second version of Theorem 4 which is useful for stability and robustness analysis:

**Theorem 6.** *Suppose $P(s) = P_{C_2}(sI - P_A)^{-1}P_B$ is SISO. Then $K(s)$ stabilizes the relative formation dynamics iff the net encirclement of $-\lambda_i^{-1}$ by the Nyquist plot of $K(s)P(s)$ is zero for all nonzero $\lambda_i$.*

*Proof.* The Nyquist criterion states that stability of the closed loop system in Theorem 4 is equivalent to the number of counterclockwise encirclements of $-1+j0$ by the forward loop $\lambda_i P(j\omega)K(j\omega)$ being equal to the number of right half plane poles of $P(s)$, which is assumed to be zero. This criterion is equivalent to the number of encirclements of $-\lambda_i^{-1}$ by $P(j\omega)K(j\omega)$ being zero. ■

In the case where $P(s)$ is MIMO, the formation can be thought of as a structured uncertainty of the type scalar time identity (see [35]) where the scalars are the Laplacian eigenvalues. More specifically, we shall write the eigenvalues as $\lambda_i = 1 + \mu_i$ and consider bounds on $\mu_i$. Suppose it is known that $|\mu_i| \leq M$ for all nonzero $\lambda_i$. If we close the loop around the unity block and leave $\mu_i I$ as an uncertainty, the resulting lower block is $C(s) = P(s)K(s)(I+P(s)K(s))^{-1}$, which is assumed to be stable. The following result from robust control theory then applies:

**Theorem 7.** *$K(s)$ stabilizes the relative formation dynamics of the MIMO vehicle $P(s)$ if*

$$\rho(C(j\omega)) < M^{-1} \quad \forall\omega \in (-\infty, \infty) \tag{18}$$

**Example 1 (Double Integrator with Time Delay).** Consider the system described in Section 2, consisting of a second order plant with time-delay and a PD control law. Figure 2 shows a formation graph and the Nyquist plot of $K(s)P(s)$ with the Laplacian eigenvalues. The black 'o' locations correspond to the eigenvalues of the graph defined by the black arcs in Figure 2, and the 'x' locations

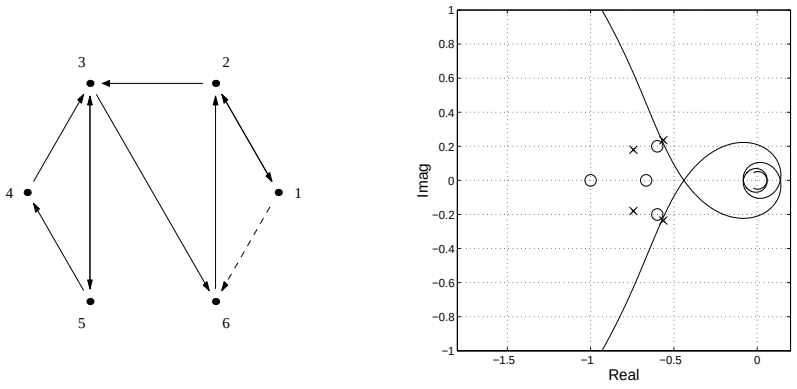


Figure 2: Formation graph and Nyquist plot.

are for eigenvalues of the graph when the dashed arc is included as well. This example clearly shows the effect the formation has on stability margins. The standard Nyquist plot reveals a system with reasonable stability margins — about 8 dB and 45 degrees. When one accounts for the effects of the formation, however, one sees that for the 'o' formation, the stability margins are substantially degraded, and for the 'x' formation, the system is in fact unstable. Interestingly, the formation is rendered unstable when additional information (its position relative to vehicle 6) is used by vehicle 1. We shall return to this point shortly.

### 4.3 Evaluating Formations via Laplacian Eigenvalues

The location of Laplacian eigenvalues has emerged as the parameter which enables formation stability to be analyzed on the local level. We now turn to the question of bounding or predicting eigenvalue location based on properties of the graph. We begin by considering simple formation structures and their eigenvalue placement. Examples of these graphs are shown in Table 1, where sample graphs, their nonzero spectra, and the locations on the Nyquist plot are shown.

1. Complete graph. The complete graph is one where every possible arc exists. In this case, the eigenvalues of a graph with $N$ vertices can be analytically determined to be zero and $1+\frac{1}{N-1}$, the latter repeated $N-1$ times. For large $N$, stabilization of the complete graph is equivalent to stabilizing an individual vehicle. Of course, a complete interconnection structure can place an enormous burden on each vehicle's sensing and computational capacities.

2. Acyclic (directed) graph. This graph has the 1 eigenvalue repeated $N$ times. This can be seen from the fact that the vertices can be ordered such that $L$ is upper triangular with ones along the diagonal. This is the "leader-follower" architecture discussed earlier. In this case, vehicle stabilization is truly a local result, since other vehicles' dynamics enter only as a disturbance. However, this architecture has drawbacks regarding disturbance rejection.

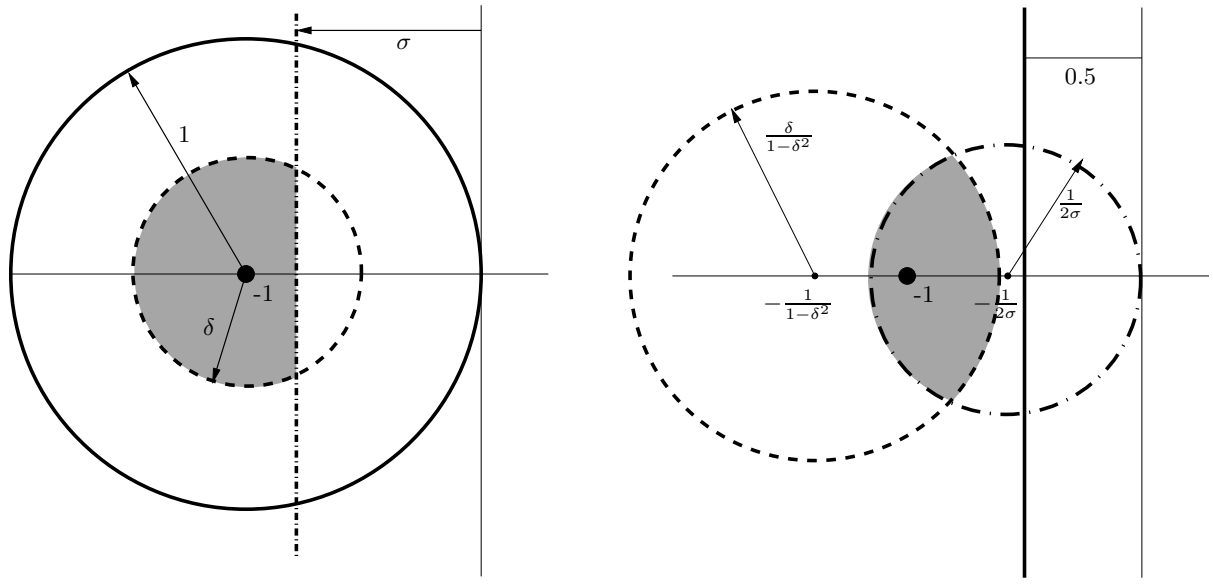


Figure 3: Inclusion Regions for $-\lambda(L)$ and $-\lambda(L)^{-1}$. Left figure shows various eigenvalue regions for $-L$ and the right figure shows the corresponding regions for $-L^{-1}$.

3. Single directed cycle. This graph is periodic, and therefore has eigenvalues at $1-e^{j(i-1)/2\pi},\ i \in [1, N]$ according to Proposition 3. These eigenvalues lie on the boundary of the Perron disk in which all the eigenvalues must lie. Note that the negative inverse of these points lie on the -0.5 vertical in the complex plane.

4. Two-cyclic undirected graph. A graph of this type would include a vehicle platoon with bidirectional position measurement. This graph will have an eigenvalue at 2, due to its periodicity, and all other eigenvalues will be real, due to the symmetry of the graph.

Figure 3 shows various eigenvalue regions for $-L$ and the corresponding regions for $-L^{-1}$. The region bounded by the solid line is the Perron disk in which all eigenvalues must lie. Its inverse is the LHP shifted by -0.5. The dashed region is a bound in the magnitude of the nonzero eigenvalues of $L$. It corresponds to a shifted circle on the right-hand side of Figure 3. Finally, the dash-dot line corresponds to a bound on the real component of the eigenvalues. The inverse of this bound corresponds to a circle which touches the origin. The shaded region represents the "desirable" region, in which the eigenvalues' locations do not differ substantially from $-1$.

If we consider the complete graph and the single directed cycle graph of Table 1 as representing two extremes — one with all eigenvalues at a single location, the other with eigenvalues maximally dispersed, we see that eigenvalue placement can be related to the rate of mixing of information through the network. When the graph is highly connected, the global component of an individual vehicle's dynamics are rapidly averaged out through the rest of the graph, and thus has only

| | | |
|---|---|---|
| 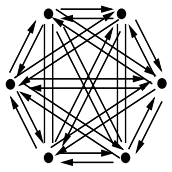 | $\lambda(L) = \{1 + \frac{1}{N-1}\}$ | 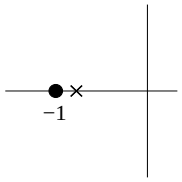  |
| 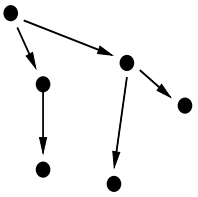 | $\lambda(L) = \{1\}$ | 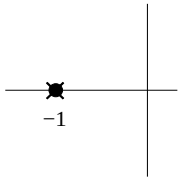  |
| 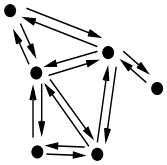 | $\lambda(L) \subset [0, 2]$ | 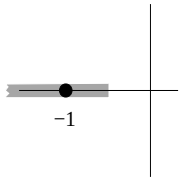  |
| 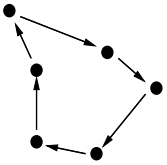 | $\lambda_i(L) = 1 - e^{\frac{2\pi j}{N}i}$ | 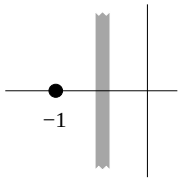  |
| 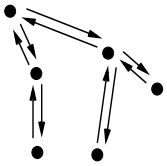 | $\lambda(L) \ni 2$ | 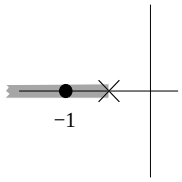  |

Table 1: Sample Graphs, Spectra, and Nyquist Locations.

a minor effect on stability. When the graph is periodic, the global component of the dynamics introduces periodic forcing of the vehicle, and the rest of the network never averages it out. This is represented on the Nyquist plot by putting the inverse eigenvalues nearer to the imaginary axis, thus diminishing stability margins.

We see that aperiodicity is a desirable property of formation interconnection topologies. With this insight, we can see why the system in Figure 2 loses stability margin when a link is added. The "solid" graph possesses two 3-cycles and two 2-cycles. When the dashed link is added, an additional 3-cycle is created, rendering the graph more nearly 3-periodic. This drives two of the eigenvalues nearer to the positions they would occupy if the graph were truly periodic, i.e., the $-0.5$ vertical. An interesting, and to the authors' knowledge, open challenge is to quantify this

insight: to define a measure of periodicity within a graph which can be correlated to bounds on the eigenvalue locations.

These results can be extended to the case where mixed absolute and relative measurements exist, such as where a subset of the vehicles sense their position relative to a target. If we consider the target as a leader of the formation with trivial (or at least decoupled) dynamics, then then the stability analysis concerns only the submatrix of $L$ containing the vehicles. In this case, the error signal of vehicle $i$ takes the form (assuming equal weighting of all measurements),

$$z_i = \frac{1}{|\mathcal{J}_i| + 1} \left( z_{i0} + \sum_{j \in \mathcal{J}_i} z_{ij} \right), \tag{19}$$

and the relevant submatrix of $L$ will still have 1 along the diagonal and off-diagonal terms equal to $-\frac{|\mathcal{J}_i|}{|\mathcal{J}_i+1|}$. Assuming all vehicles have access to the target, then $\rho(G) < 1$ (Theorem 2), so $L$ does not have a zero eigenvalue. This corresponds to the fact that unobservability of bulk formation motion is no longer relevant when the formation can view the target. From this perspective, the presence of absolute measurements tightens the bound on $\lambda(L)$, which improves the stability picture. However, it does not guarantee that individual eigenvalues will not be nearer to the bound than they were in the case where only relative measurements where present.

As discussed earlier, significant efforts have been made by graph theorists to relate eigenvalue location to various graph-theoretic properties. These results were largely derived for undirected graphs, whose eigenvalues are real and can be bounded using variational techniques. For directed graphs, the problem is more challenging. Most of the work cited earlier regarding eigenvalue bounding focuses on the algebraic connectivity and its relationship to substructures in the graph. As we have seen, the algebraic connectivity does not directly impact stability margins. Of greater interest to this application are bounds such as $\lambda$ in Figure 3, which identify the region in which the majority of eigenvalues are located, with the possible exception of isolated eigenvalues near the origin. Examining the structure of the cycles in the graph may lead to interesting results in this area.

# 5 Information Flow in Vehicle Formations

In Section 2, we show via example how the communication topology impacts performance as well as stability. The absence of a centralized controller causes individual vehicles to follow contradictory trajectories. As we discuss in the introduction, traditional methods for supplying a vehicle formation with an agreed-upon leader presume the existence of a communication and computation infrastructure which facilitates real-time determination of the formation leader.

In this section, we explore a paradigm for information exchange which enables the vehicles to jointly determine a virtual formation leader which does not presuppose any communication

topology. Our goal is to derive an information exchange policy whose stability and convergence are robust to changes in the graph. The stability analysis tools developed in the previous section will be useful in this development, as will theorems from Perron-Frobenius theory developed in Section 3.2.

In the previous section, we assume that sensed information was available instantaneously, and we used a continuous-time model of the vehicle dynamics. In this section, we assume that information takes a fixed time $T$ to travel between vehicles. To facilitate analysis, we also model each vehicle as a discrete time dynamical system:

$$\begin{aligned} x^i_{k+1} &= P_A x^i_k + P_B u^i_k \\ y^i_k &= P_C x^i_k + P_D u^i_k \end{aligned} \tag{20}$$

where $k$ is the time step of duration $T$ and $i$ is the vehicle index. The error signal is given in Equation (8). Note that the stability results of Section 4.2 can be reproduced for discrete time systems by plotting the response of the discrete-time transfer function for $z = e^{j\omega}$ and applying the Nyquist criterion.

Broadly speaking, any decentralized formation control system consists of vehicles receiving a transmission from other vehicles and performing some computation using that information, information from previous transmissions, and sensed information. Each vehicle then transmits the results of their computation to other vehicles. We can view this process as a discrete-time dynamical system where the states are the information at each vehicle. This can be generically represented as

$$p^i_{k+1} = f(p^i_k, p^i_{k-1}, \ldots, \{p^j_k, p^j_{k-1}, \ldots | j \in \mathcal{J}^T_i\}, z^i_{k+1}, z^i_k \ldots), \tag{21}$$

where $\mathcal{J}^T_i$ is the set which determines the transmitted information topology. For the remainder of this paper, we assume that the sensed and transmitted information graph are identical, and omit the superscript. Our approach is to shape this dynamical system to ensure that its evolution has the desired stability and convergence properties. We term this approach *information flow*.

The information flow law we investigate mimics the structure of the sensed information flow, taking the following form:

$$p^i_{k+1} = \sum_{j \in \mathcal{J}_i} p^j_k + (y^i_k - y^j_k) \tag{22}$$

or, in vector form:

$$p_{k+1} = G_{(m)} p_k + L_{(m)} y_k, \tag{23}$$

where $G_{(m)}$ and $L_{(m)}$ are the directed adjacency matrix and Laplacian of the graph, as defined in Section 3.2, dimensioned compatibly with the measurement vector $y^i_k$ whose dimension is denoted $m$. Henceforth, we shall assume that $m = 1$, and dispense with the extra notation. As discussed in the previous section, the commutation result of Lemma 5 implies that the dimension of $y$ is not

relevant. For the information flow laws to be derived, one can replicate all the results by replacing the given transfer functions with the same transfer function repeated $m$ times along the diagonal.

## 5.1 Convergence of the Information Flow Loop

Let us explore this information flow paradigm in some detail. The information flow component is a discrete time dynamical system which, as discussed above, is neutrally stable due to the Perron root of $G$. We begin by determining the steady-state behavior of the information flow loop. In preparation, we introduce some definitions and related lemmas.

Let $e_r$ denote the right Perron eigenvector of $G$, and $e_l$ its left Perron eigenvector, normalized such that $e_r^T e_l = 1$. If $G$ is irreducible, both $e_r$ and $e_l$ are positive (Theorem 2), so such a scaling must exist. Let $E = e_r e_l^T$. The following relationships between $G$ and $E$ are known to be true: (See [20], p. 498, and recall that the Perron eigenvalue is 1.)

**Lemma 8.** $G^j = E + (G - E)^j$.

**Lemma 9.** *The eigenvalues of $G - E$ are the eigenvalues of $G$ with the Perron eigenvalue replaced with a zero eigenvalue.*

We now state and prove the following theorem:

**Theorem 10.** *Suppose the directed graph $\mathcal{G}(G)$ is strongly connected and aperiodic, and let the input $y_k$ be fixed in time. The steady state value of the dynamical system in Equation (23), when $p_0 = 0$, is*

$$p_{ss}^i = y^i - \sum_{j=1}^{N} e_l^j y^j \tag{24}$$

*where $e_l^i$ is the $i$th element of the left Perron eigenvector of $G$, scaled so that $\sum e_l^i = 1$.*

*Proof.* Consider the evolution of Equation (23):

$$p_k = G^k p_0 + \left( \sum_{j=0}^{k} G^j \right) Ly. \tag{25}$$

We assume that $p_0 = 0$, and we wish to find $p_{ss} = \lim_{k\to\infty} p_k$, if such a limit exists. Substituting into Equation (25) via Lemma 8, we have

$$p_k = \left( \sum_{j=0}^{k} E^j + (G - E)^j \right) Ly. \tag{26}$$

Recalling that $E = e_r e_l^T$, and that $L$ shares eigenvectors with $G$, we see that $e_r$ and $e_l$ are the eigenvectors of $L$ corresponding to the zero eigenvector. Therefore, $EL = e_r e_l^T L = e_r 0 = 0$, and

we can rewrite $p_k$ as

$$p_k = \left( \sum_{j=0}^{k} (G-E)^j \right) Ly. \tag{27}$$

Because $G$ is assumed irreducible and aperiodic, all non-Perron eigenvalues of $G$ have modulus strictly less than one (Theorem 3). Therefore, by Lemma 9, we see that $\rho(G-E) < 1$. The infinite expansion of $p_{ss}$ therefore converges ([20], p. 301) and can be written as follows:

$$\begin{aligned} p_{ss} &= \left( \sum_{j=0}^{\infty} (G-E)^j \right) Ly \\ &= (I - G + E)^{-1} Ly \\ &= (L+E)^{-1} Ly \\ &= (L+E)^{-1}(L+E-E)y \\ &= (I - (L+E)^{-1}E)y. \end{aligned} \tag{28}$$

Now $Le_r = 0$, and $Ee_r = (e_r e_l^T)e_r = e_r(e_l^T e_r) = e_r$, so $(L+E)e_r = e_r \Rightarrow (L+E)^{-1}e_r = e_r$, and hence

$$\begin{aligned} p_{ss} &= (I - (L+E)^{-1} e_r e_l^T)y \\ &= (I - e_r e_l^T)y \\ &= (I - E)y. \end{aligned} \tag{29}$$

The eigenvector $e_r$ is known to be $1^T$. The eigenvector $e_l$ is positive, and is scaled such that $\sum e_l^i = 1$. The columns of $E$ are therefore constant, and the rows are each $e_l^T$. Therefore, Equation (29) can be written

$$p_{ss}^i = y^i - \sum_{j=0}^{N} e_l^j y^j. \tag{30}$$

■

The information flow loop therefore has the effect of having the formation track the formation center, where the center is defined according to a weighting given by the graph. In this architecture, the weighting cannot be chosen, though in principle it could be set by unevenly weighting the information when performing the averaging. However, this would require global knowledge of the graph, which is assumed not to be available.

Theorem 10 demonstrates both stability and convergence of an information flow law given a constant input and aperiodicity of the graph. We now consider the a more general information flow law which enables the designer to shape the dynamics of the information flow:

$$\begin{aligned} q_{k+1} &= \textstyle\sum_{j=0}^{R} a_j q_{k-j} + G \sum_{j=0}^{R} b_j q_{k-j} + L y_k \\ p_k &= \textstyle\sum_{j=0}^{R} c_j q_{k-j}. \end{aligned} \tag{31}$$

In this version, we are computing our current information using information from previous time steps as well as information received from other vehicles through a filter. This formulation can also be used to account for the presence of additional delays in data transmission. In this case, we prove separate stability and convergence theorems. We begin by checking stability of the information flow law using the tools from Section 4.

**Theorem 11.** *The system in Equation (31) is (neutrally) stable if the transfer function*

$$F(z) = \frac{\sum_{j=0}^{R} b_j z^{R-j}}{z^{R+1} - \sum_{j=0}^{R}(a_j + b_j) z^{R-j}} \tag{32}$$

*is (neutrally) stable and its Nyquist plot avoids encirclement of the negative inverse of any of the nonzero eigenvalues of $L$.*

*Proof.* We can take the $z$-transform of Equation (31), setting aside the input, and rewrite it as follows:

$$\begin{aligned} zq(z) &= \sum_{j=0}^{R} a_j z^{-j} q(z) + \sum_{j=0}^{R} b_j G z^{-j} q(z) \\ &= \sum_{j=0}^{R} (a_j + b_j) z^{-j} q(z) - \sum_{j=0}^{R} b_j L z^{-j} q(z) \end{aligned}$$

or, if we collect terms not including $L$ and multiply both sides by $z^R$,

$$q(z) = -\frac{\sum_{j=0}^{R} b_j z^{R-j}}{z^{R+1} - \sum_{j=0}^{R}(a_j + b_j) z^{R-j}} L q(z). \tag{33}$$

The transfer function in the above equation is $\hat{F}(z)$, and this equation is equivalent to the lower loop shown in Figure 4. This block diagram has the same structure as the system of vehicle formations examined in Section 4, where it was shown in Theorems 4 and 6 that the stability of this system is given by the Nyquist criterion stated above. Because one set of eigenvalues of this system corresponds to the open-loop dynamics, this system can be at best neutrally stable if $F(z)$ is itself neutrally stable. ■

We now turn to the steady-state performance of the information flow law. We assume that $c_j = b_j$, which is useful in the stability proofs of Section 5.2, and which implies that each vehicle need only transmit $p_k = \sum_{j=0}^{R} b_j q_{k-j}^i$ to its neighbors. We also assume that $F(z)$ has all poles on the interior of the unit circle with the possible exception of a simple pole at 1. Finally, we assume that the polynomial $\sum_{i=0}^{R} a_i z^{R-i}$ has roots in the interior of the unit circle.

**Theorem 12.** *If $F(z)$ stabilizes $L$ in the sense of Theorem 11, and under the above assumptions,*

$$p_{ss} = c\left(I - cE - (1-c)\left(I - c(G-E)\right)^{-1} G\right) y \tag{34}$$

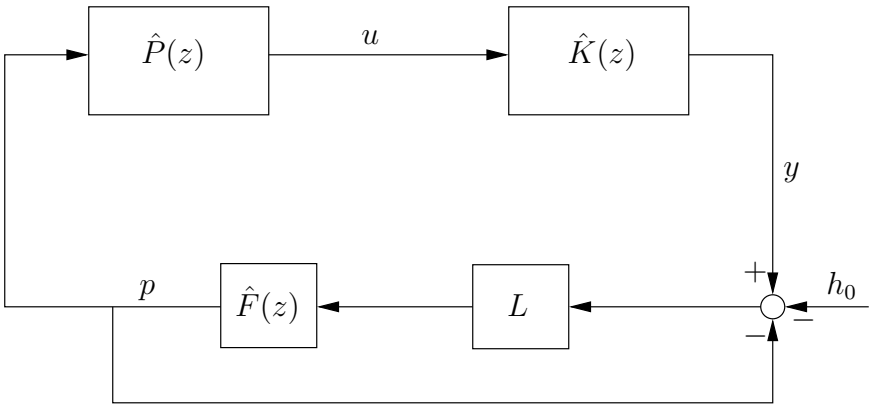


Figure 4: Block Diagram of Information Flow in the Loop.

*where* $a = \sum_{j=0}^{R} a_j$, $b = \sum_{j=0}^{R} b_j$, *and* $c = \frac{b}{1-a}$.

*Proof.* The proof is a lengthier version of the proof for Theorem 10, and can be found in [13]. ■

Note that $c = 1$ corresponds to $a + b = 1$, which implies that the system has a pole at 1. When $c = 1$, we recover the steady-state result of Theorem 10, only we now see it to be true for any information flow filter with a pole at 1 (and which stabilizes the graph). When $c < 1$, the steady-state is offset by an additional term. Note that when $c = 1$, the vehicles all agree on the location of the formation center (expressed in each vehicle's coordinates), while when $c < 1$, they do not. We can say that when $c = 1$, the vehicles achieve *consensus* on formation center. From this perspective, having $c = 1$ appears to be a desirable property of the information flow filter. However, when $c = 1$, the system is only neutrally stable. The reason the filter converges to a steady state is because the input passed through $L$, whose kernel is equal to the Perron eigenvector of $G$. However, the presence of noise or sensor errors has the potential to introduce drift. Additionally, the eigenvalue at 1 means that old information never decays out, rendering the system sensitive to initial conditions. Of course, the initial conditions of the information flow law can be set (or reset) by the vehicle, assuming the existence of a protocol which guaranteed that this could be done without disrupting the formation.

**Example 2.** To understand the effects of shaping the information flow, we consider two examples. The first filter is in Equation (23). In this case, following Equation (32), $F_1(z) = \frac{1}{z-1}$. The second

filter is given by

$$p_{k+1} = 1.0625p_k - 0.2313p_{k-1} + 0.1875Gp_k - 0.0188Gp_{k-1} \quad (35)$$

$$q_k = 0.1875p_k - 0.0188p_{k-1}. \quad (36)$$

This corresponds to $F_2(z) = \frac{0.1875(z-0.1)}{(z-0.25)(z-1)}$. The pole at 1 means that $c = 1$ in both cases. Figure 5 shows the Nyquist plot for these two filters. The first lies along the $-0.5$ vertical. Points on that line correspond to periodic graphs (see Section 3.3), which confirms Theorem 10. The second lies entirely to the right of the $-0.5$ vertical. Recalling from Section 4.3 that the Nyquist plot points generated by the Laplacian, $-\lambda_i(L)^{-1}$, all must lie on or to the left of this vertical, we conclude that this information flow law stabilizes any graph.

Figures 5,6 shows the response of the two filters to a step response for a sparsely connected graph. While both settle in approximately 0.5 sec (using a time step of 0.02 sec), the first filter exhibits ringing due to the proximity of the closed loop poles to the unit circle. The second filter has a much smoother response. We see how the information flow filter can be designed to achieve desirable responses and robustness to uncertainty in the graph.

We note in passing that this approach is easily extended to the case where some vehicles can sense their position relative to the target or to an absolute reference frame. In that case, the desired graph structure is that the target be the sole leader component of the graph to which all other vehicles have access. In this case, the Perron eigenvector is $[1, 0, 0, \ldots]^T$ (see [13]), meaning each vehicle's information converges to its position relative to the target — a desirable result. Of course, the target is not transmitting any information, so the vehicles that sense the target must generate the information the target would be transmitting. Since the target is by definition at its desired location, the target's transmitted information is just zero.

### 5.2 Information Flow in the Loop

The information flow filter supplies each vehicle with the information it cannot sense: a formation center about which to do control. The information $p$ represents the position of the virtual leader relative to each vehicle, and is therefore the logical input to the controller $K(z)$. A block diagram for this architecture is shown in Figure 4. As before, we can analyze stability with respect to uncertainties in the graph by isolating $L$ and applying the Nyquist criterion as in Theorem 6. In this case, one determines stability by analyzing the Nyquist plot of

$$F(z)(1 + K(z)P(z)). \quad (37)$$

For a given plant and controller, the information flow loop can be designed to provide desirable margins. However, care must be taken in interpreting the stability margins derived from this plot.

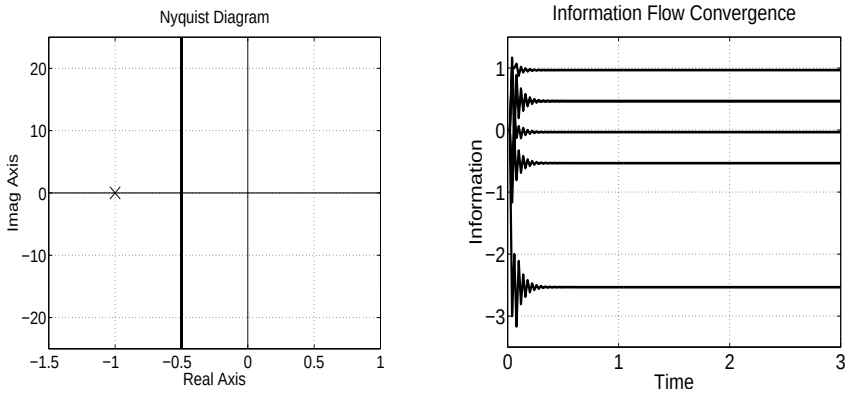


Figure 5: Information Filter Nyquist Plots.

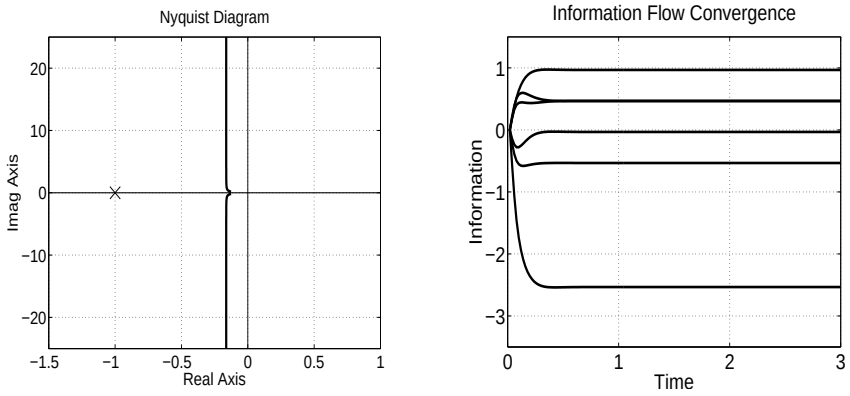


Figure 6: Information Filter Convergence.

The gain and phase margins of this plot do not correspond to uncertainties in the plant in the typical fashion due to the location of $P(z)$ in the transfer function. Instead, they correspond more directly to uncertainties in $L$. Small variations in $P(z)$ can produce unexpected perturbations of the Nyquist plot. A reasonable design methodology is to design $K(z)$ to stabilize $P(z)$, without regard to the graph (remember that stabilizing the formation is never easier than stabilizing an individual vehicle) and then design $F(z)$ to stabilize $L$. However, the coupling between the dynamics of the two can produce unexpected results. In this section, we explore a means to improve this situation.

The information flow algorithm presented earlier is necessarily reactive; it does not anticipate the motion of the cluster. A logical means of improving performance is to supply the information flow loop with feedforward information regarding the expected motion of the formation. Recalling that the information represents an averaged position of the vehicles' positions, a logical choice for a feedforward signal is the anticipated change in vehicle position. This can be calculated by using each vehicles' control signal $u(z)$ as the input to a model of the plant, denoted $\tilde{P}(z)$, and

differencing that. The resulting signal

$$w^i(z) = (1 - z^{-1})\tilde{P}(z)u^i(z) \tag{38}$$

is then transmitted in addition to the signal $q(z)$ and used by each vehicle as a correction term to $p$. For example, we would replace Equation (23) with the following information flow law:

$$\begin{aligned} q_{k+1} &= G(q_k + w_k) + Ly_k \\ p_k &= q_k + w_k \end{aligned} \tag{39}$$

In this case, the transmitted quantity is $p_k^i = q_k^i + w_k^i$, as is clear from is premultiplication by $G$. Of course, this feedforward correction term is only current if the control signal is delayed by a time step before application to the plant to allow a time step for the information to reach the other vehicles. Alternatively, each vehicle could delay the use of its sensed information until it receives the transmitted information from that vehicle.

To allow for information flow laws more general than Equation (38), we will let $w(z)$ take on the more general form

$$w(z) = H(z)\tilde{P}(z)u(z). \tag{40}$$

The information flow block diagram for this architecture is shown in Figure 7. When $H(z)$ is chosen properly, the following result can be derived:

**Theorem 13.** *Choose $H(z)$ to be*

$$H(z) = \frac{1}{F(z) + 1}, \tag{41}$$

*and suppose the feedback interconnection of $P(z)$ and $K(z)$ is well-posed. Then the relative formation dynamics are stabilized if and only if F(z) stabilizes L in the sense of Theorem 11 and $K(z)$ stabilizes $P(z)$.*

*Proof.* By construction, $F(z)$ is biproper. Using our definition of $F(z)$, we can write $H(z)$ as

$$H(z) = \frac{z^{R+1} - \sum_{j=0}^{R}(a_j + b_j)z^{R-j}}{z^{R+1} - \sum_{j=0}^{R} a_i z^{R-j}}. \tag{42}$$

Note that $H(z)$ is stable due to the assumptions of Theorem 11.

We prove the presence of a separation principle for the system of equations, through the use of a transformation of coordinates that isolates the subsystems whose stability implies stability of the overall system. To do this, we first present the system of equations in state-space form. The state-space equations of motion for the plant are given in Equation (20). The predictor $\tilde{P}(z)$ is presumed to be identical to the plant $P(z)$, and has the same equations of motion with $x, y$ replaced by $\tilde{x}, \tilde{y}$. The dynamics of the controller will be represented as

$$\begin{aligned} v_{k+1}^i &= K_A v_k^i + K_B p_k^i \\ u_k^i &= K_C v_k^i + K_D p_k^i. \end{aligned} \tag{43}$$

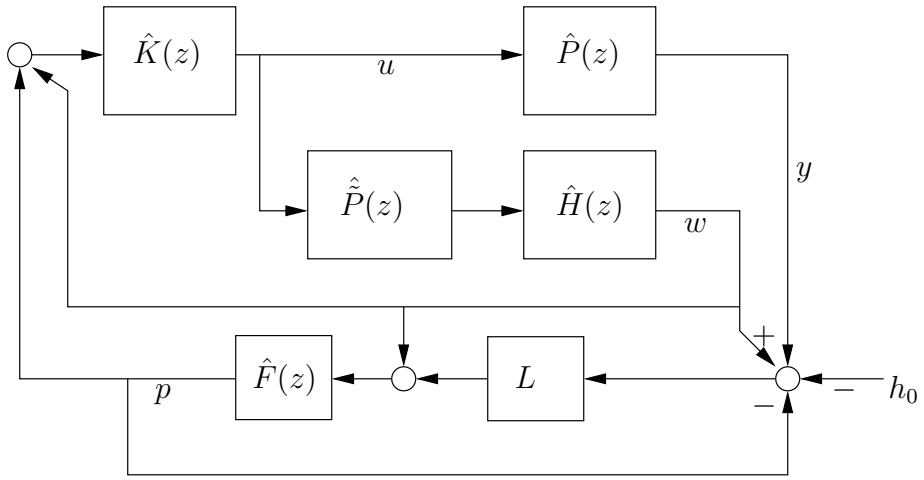


Figure 7: Block Diagram of Information Flow with Feedforward Correction.

The information flow filter $F(z)$ is defined as found in Equation (31), but with the feedforward correction term added:

$$\begin{array}{rcl} q_{k+1} & = & \sum_{j=0}^{R} a_j q_{k-j} + G\left(\sum_{j=0}^{R} b_j q_{k-j} + w_k\right) + L y_k \\ p_k & = & \sum_{j=0}^{R} b_j q_{k-j} + w_k. \end{array} \tag{44}$$

Once again, it should be clear from the position of the quantity $p_k = \sum_{j=0}^{R} b_j q_{k-j} + w_k$ that it is the information which is transmitted by each vehicle.

Finally, the state space representation of the feedforward correction term, found in Equation (42), is

$$\begin{array}{rcl} r^i_{k+1} & = & \sum_{j}^{R} a_j r^i_{k-j} + \tilde{y}^i_k \\ w^i_k & = & -\sum_{j}^{R} b_{k-j} r^i_k + \tilde{y}^i_k. \end{array} \tag{45}$$

To simplify the representation of Equations (44) and (45) in state-space notation, we introduce the following notation. Let

$$H_A = \begin{pmatrix} 0 & 1 & \cdots & 0 \\ \vdots & \vdots & \ddots & \vdots \\ 0 & 0 & \cdots & 1 \\ a_R & a_{R-1} & \cdots & a_0 \end{pmatrix}, \tag{46}$$

let

$$H_B = \begin{bmatrix} 0 & 0 & \cdots & 1 \end{bmatrix}^T, \tag{47}$$

and let

$$H_C = \begin{bmatrix} b_R & \cdots & b_0 \end{bmatrix}, \tag{48}$$

where $H_B$ is dimensioned compatibly with $H_A$. For the information flow law and feedforward term, we use $\bar{q}^i$ to denote $[q^i_{k-R}, q^i_{k-R+1}, \ldots, q^i_k]^T$, and similarly for $\bar{r}$. The state-space representation of Equation (44) can thus be represented as

$$\begin{aligned} \bar{q}_{k+1} &= \widehat{H}_A \bar{q}_k + \widehat{H}_B G(\widehat{H}_C \bar{q}_k + w_k) + \widehat{H}_B L y_k \\ p_k &= \widehat{H}_C \bar{q}_k + w_k \end{aligned} \tag{49}$$

and of Equation (45) as

$$\begin{aligned} \bar{r}_{k+1} &= \hat{H}_A \bar{r}_k + \hat{H}_B \tilde{y}_k \\ w_k &= -\hat{H}_C \bar{r}_k + \tilde{y}_k. \end{aligned} \tag{50}$$

If one solves Equations (20), (43), (49), and (50) for the states, the resulting system of equations is

$$X_{k+1} = \Psi X_k, \tag{51}$$

where $X_k = [x_k, v_k, \tilde{x}_k, \bar{r}_k, \bar{q}_k]$ and

$$\Psi = \begin{pmatrix} \widehat{P}_A & \widehat{P}_B\Delta\widehat{K}_C & \widehat{P}_B\widehat{K}_D\Delta\widehat{P}_C & -\widehat{P}_B\widehat{K}_D\Delta\widehat{H}_C & \widehat{P}_B\widehat{K}_D\Delta\widehat{H}_C \\ 0 & \widehat{K}_A + \widehat{K}_B\widehat{P}_D\Delta\widehat{K}_C & \widehat{K}_B\Delta\widehat{P}_C & -\widehat{K}_B\Delta\widehat{H}_C & \widehat{K}_B\Delta\widehat{H}_C \\ 0 & \widehat{P}_B\Delta\widehat{K}_C & \widehat{P}_A + \widehat{P}_B\widehat{K}_D\Delta\widehat{P}_C & -\widehat{P}_B\widehat{K}_D\Delta\widehat{H}_C & \widehat{P}_B\widehat{K}_D\Delta\widehat{H}_C \\ 0 & \widehat{H}_B\widehat{P}_D\Delta\widehat{K}_C & \widehat{H}_B\Delta\widehat{P}_C & \widehat{H}_A - \widehat{H}_B\widehat{P}_D\widehat{K}_D\Delta\widehat{H}_C & \widehat{H}_B\widehat{P}_D\widehat{K}_D\Delta\widehat{H}_C \\ \widehat{H}_B L\widehat{P}_C & \widehat{H}_B\widehat{P}_D\Delta\widehat{K}_C & \phi\widehat{P}_C & -\phi\widehat{H}_C & \widehat{H}_A + \phi\widehat{H}_C \end{pmatrix} \tag{52}$$

where $\phi = \widehat{H}_B(\widehat{P}_D\widehat{K}_D\Delta + G)$, and $\Delta = (I - \widehat{P}_D\widehat{K}_D)^{-1}$, which is invertible by assumption of well-posedness of the interconnection. If we apply the transformation

$$T = \begin{pmatrix} I & 0 & 0 & I & 0 \\ 0 & 0 & I & 0 & 0 \\ 0 & 0 & 0 & I & 0 \\ 0 & I & 0 & 0 & I \\ 0 & 0 & 0 & 0 & I \end{pmatrix} \tag{53}$$

to the system matrix, we recover the matrix

$$T^{-1}\Psi T = \begin{pmatrix} \boxed{\widehat{P}_A} & 0 & 0 & 0 & 0 \\ -\widehat{H}_B L\widehat{P}_C & \boxed{\widehat{H}_A + \widehat{H}_B G\widehat{H}_C} & 0 & 0 & 0 \\ 0 & -\widehat{K}_B\Delta\widehat{H}_C & \boxed{\widehat{K}_A + \widehat{K}_B\widehat{P}_D\Delta\widehat{K}_C} & \boxed{\widehat{K}_B\Delta\widehat{P}_C} & 0 \\ 0 & -\widehat{P}_B\widehat{K}_D\Delta\widehat{H}_C & \boxed{\widehat{P}_B\Delta\widehat{K}_c} & \boxed{\widehat{P}_A + \widehat{P}_B\widehat{K}_D\Delta\widehat{K}_C} & 0 \\ \widehat{H}_B L\widehat{P}_C & -\phi\widehat{H}_C & \boxed{\widehat{H}_B\widehat{P}_D\Delta\widehat{K}_C} & \boxed{\widehat{H}_B\Delta\widehat{P}_C} & \boxed{\widehat{H}_A} \end{pmatrix}. \tag{54}$$

Stability of the system is equivalent to stability of the blocks along the diagonal. The first, $P_A$, is neutrally stable by assumption. The assumption that the information flow law stabilizes the graph is equivalent to the second block, $H_A + H_B G H_C$, being stable. The third block along the diagonal, which comprises the third and fourth columns/rows, is stable if $K(z)$ stabilizes $P(z)$. (The reader will verify that this is the matrix derived when $K(z)$ and $P(z)$ are interconnected directly via feedback.) The final block represents the states of $H(z)$, which is stable by the assumption in Theorem

11. We thus derive a separation principle for our formation which demonstrates that design of the individual vehicle controller $K(z)$ and the information flow filter $F(z)$ can be decoupled. ■

**Remarks** Equation (54) can be interpreted in the following way. The first set of states are open-loop copies of the vehicles' dynamics, and represent mismatches in initial conditions between the predictor and the actual vehicle. The second set is identical to the dynamics of Equation (31), whose stability and convergence properties were studied above. The output of this set of states acts as a reference to $N$ more copies of the vehicle dynamics in feedback interconnection with the local controllers, found in the third and fourth rows. We see, therefore, that the effect of this architecture is to supply the local controllers with a reference signal which, if implemented properly, represents the error of that vehicle relative to a common reference trajectory whose dynamics obey the open loop dynamics of an individual vehicle. The final set of states represent the feedfoward component. These states are unobservable in the motion of the vehicles, but are stable by design.

Several observations can be made regarding implementation. The first is that the motion of the formation is sensitive to mismatches between initial conditions of the vehicle and predictor. This can lead to drift of the cluster if the mismatch is in velocities. It should be possible to improve upon this through the use of an observer which will prevent the vehicle and predictor from diverging. Another solution is to initialize the predictor using earlier measurements.

The second is that if $c \neq 1$, meaning the information flow loop does not converge to a common reference, then the vehicles' final positions will incorporate those errors as well (although the system is stable in this case as well). The position of the vehicles will also depend on the ability of the information flow filter to track the natural motion of the vehicles. When the natural motion of the vehicles is at rest, we have seen that it achieves a proper steady state when $c = 1$. When the natural motion is secular drift or oscillation (corresponding to poles at the origin or along the $j\omega$ axis), the quality of the reference signal will depend on the ability of the information flow filter to track signals at the relevant frequencies.

We also note that the model of the plant $\tilde{P}(z)$ is not an observer, but a predictor of vehicle motion. The zero at 1 in $H(z)$ corresponds to differencing the input, which generally amplifies signal noise. However, the input to $H(z)$ is derived by integrating $u(z)$, so no net differencing takes place in the filter. In fact, it is possible to compress $P(z)$ and $H(z)$ into a single filter, but it is easier not to do so when proving stability.

Finally, we note that unlike the results of the previous section, this separation principle does *not* rely on the vehicles having identical plants or controllers. It merely relies on each vehicle's predictor matching the vehicle dynamics and on each vehicle implementing the same information flow and feedfoward correction computation. This eliminates a significant obstacle to implementation. A

minor consequence is that when the vehicles have the same dynamics, the bulk motion of the formation itself obeys the dynamics of a single vehicle, while when the vehicles have different dynamics, that motion will be more complex.

**Example 3 (Formation Acquisition).** We return to the example with which we began in Section 2. If the information flow law together with feedforward compensation is enabled, the vehicles follow the trajectories shown on the left in Figure 8. The trajectories are smoother, but still show some curving due to action of the control law prior to convergence of the information flow law. The right-hand figure shows the trajectories followed by the vehicles when the information flow law is enabled one second prior to enabling the control loop. In this case, the vehicles follow straight lines to their targets. Note that the formation center is identical in the two cases despite the differing trajectories. This is due to the decoupling of the information flow law from expected formation motion.

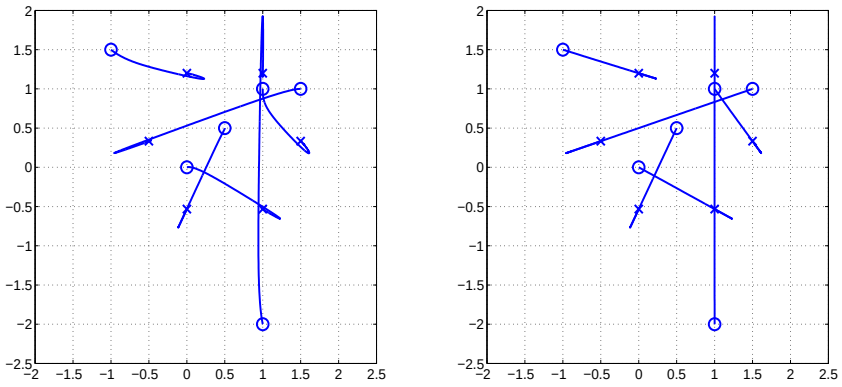

Figure 8: Hexagon acquisition with information flow using no information pre-convergence (left) and using one second of information preconvergence (right).

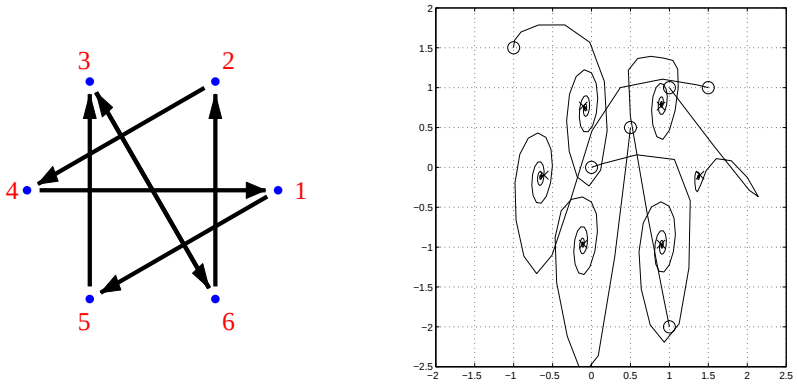


Figure 9: Communication topology and hexagon acquisition using only sensed infromation.

If we presume a different communication topology, we see the role the information flow law plays

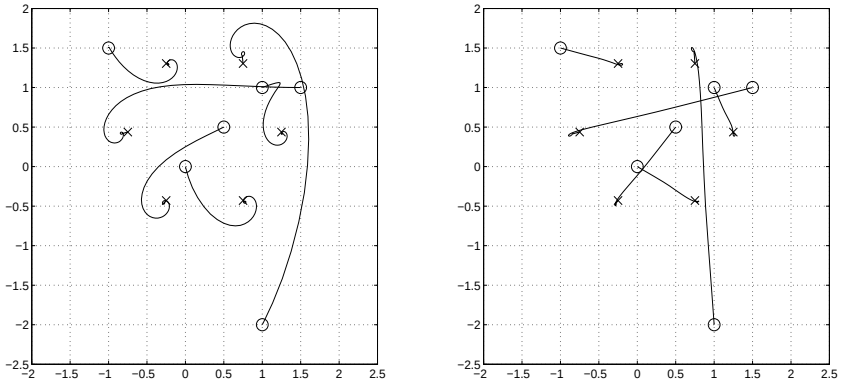

Figure 10: Hexagon acquisition with information flow using no information pre-convergence (left) and using one second of information preconvergence (right).

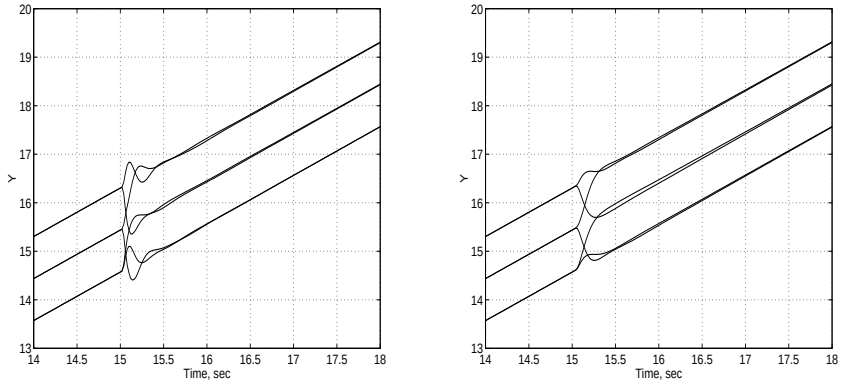


Figure 11: The $y$-axis transients of formation reconfiguration, without information flow (left) and with information flow (right).

in decoupling formation dynamics and vehicle dynamics. Figure 9 shows a different topology and the formation acquisition trajectories followed using only sensed information. The transients are worse in this example because the Laplacian eigenvalues are nearer to instability. Figure 10 shows the trajectories when information flow is employed. Again, the left hand figure shows the trajectories when vehicle control and information flow are enabled simulatneously, and the right hand figure shows the trajectories when information flow is enabled earlier. Once again, the information flow renders then formation response largely insensitive to the communication topology.

**Example 4 (Formation reconfiguration).** In this example, the formation is already in a hexagonal formation and traveling in the positive $y$ direction, when a command is issued for the formation to rotate counterclockwise. The transients for the motion of each vehicle in the $y$ direction are shown on the left in Figure 11 for the case where information flow is disabled and on the right for the case where information flow is enabled. The use of information flow reduces the transients

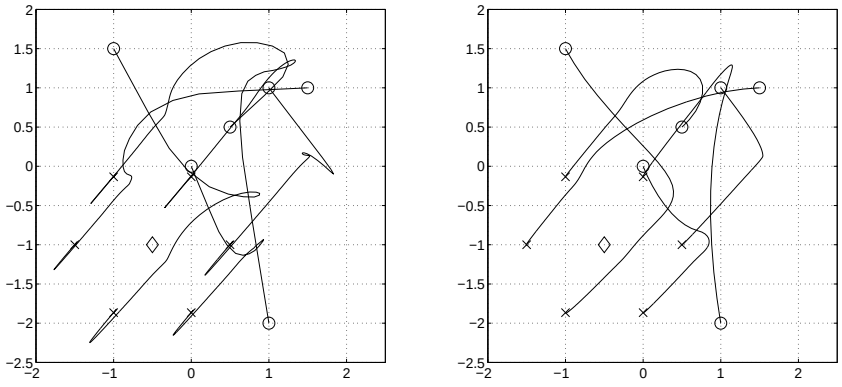

Figure 12: Target acquisition with no information flow (left) and with information flow (right)

associated with the reconfiguration as it did with the formation acquisition.

**Example 5 (Target Acquisition).** In this example a target becomes visible to a single vehicle as the formation is acquiring the hexagon. The vehicle which views the target includes that information as described earlier, and attempts to bring the vehicles into formation with the target at the center of the hexagon. The left plot in Figure 12 shows the formation motion with information flow disabled. In this case, the vehicle which can view the target has to reconcile conflicting information: its position relative to the target and relative to the other vehicles, which are unaware of the targets existence. This causes the formation to overshoot the target, marked with a diamond, and to slowly settle into the desired position.

The right plot in Figure 12 shows the same situation with information flow enabled. In this case, the information flow loop disseminates the target information to the other vehicles, causing the information loop to treat the target as the formation leader and use its position as the common reference. In this case, the formation gracefully changes course and quickly acquires the target.

**Example 6 (Satellite Reconfiguration).** We now consider an example from a different domain: relative satellite motion. This problem is motivated by missions such as the TechSat 21 mission, in which a collection of small satellites are used to distributed aperature sensing.

The relative motion of a second satellite about a reference satellite can be approximating by linearizing the Keplerian orbital mechanics about the reference trajectory. These equations are known as Hill's equations due to Hill's study of lunar motion [19] and as the Clohessy-Wiltshire equations due to their work on orbital rendezvous [7]. The equations of motion about a circular reference orbit are

$$\begin{aligned} \ddot{x} &= 3n^2 x + 2n\dot{y} + a_x \\ \ddot{y} &= -2n\dot{x} + a_y \\ \ddot{z} &= -n^2 z + a_z \end{aligned} \tag{55}$$

where $x$ point in the radial direction, $y$ along track, and $z$ out of plane. The orbit rate is given by $n$.

The vector $[a_x,\ a_y,\ a_z]^T$ represents external accelerations, either due to environmental disturbances or applied thrust. The equations, when solved, reveal families of periodic orbits about the origin as well as secular drift along $y$. The periodic solutions include a $2 \times 1$ inclined ellipse whose projection onto the Earth (the $yz$ plane) is a circle. The ground track of these satellites remains fixed relative to one another and rotates at orbit rate. These orbits are attractive for space-based interferometry, such as the TechSat21 mission, and were part of the impetus for exploring missions of this type [21]. We also note that interferometry requires accurate knowledge of relative satellite position, but drift in absolute position is more tolerable. Hill's equations are often used as a coarse model for relative satellite motion despite the absence in the model of external forces and perturbations of Earth's gravitational field.

Note that the $xy$-dynamics are decoupled from the $z$-dynamics. Setting $n = 1$, a family of unforced solutions to the $xy$ dynamics is given by

$$\begin{aligned} x(t) &= A\cos(t+\phi) \\ y(t) &= y_0 - 2A\sin(t+\phi). \end{aligned} \tag{56}$$

Consider a set of six satellites, evenly spaced initially along the $y$-axis, that are asked to take up stations along a Hill's ellipse given by $A = 1$ at evenly spaced $\phi$. Each satellite can measure the full relative states of a subset of other satellites, and an LQR controller has been designed. The offset $h_{i0}$ is given by Equation (56) and its derivative, with $\phi = \frac{\pi i}{3}$, and $y_0 = 0$. We begin by designing the information flow law. In this case, the reference signal which the vehicles must determine follows a periodic trajectory. To ensure good tracking, we place poles of the information flow law at the (discretized) frequency locations, along with a pole at 1 so that the $c = 1$ condition is satisfied. A candidate information flow law is given by

$$F(z) = \frac{z^2 - 1.6575z + 0.7225}{z^3 - 2.9975z^2 + 2.9975z - 1}. \tag{57}$$

The Nyquist plot for this information flow law is found in the leftmost plot of Figure 13. In this case, the desire for good tracking of the reference signal places limits on the range of graphs which the information flow law stabilizes. Nonetheless, the encircled region of Figure 13, which offsets the encirclement at infinity, leading to zero net encirclements, gives reasonable latitude around the $-1$ point. Once $F(z)$ is designed, then the feedforward term $H(z)$ is derived automatically. The center plot in Figure 13 shows the reference signal supplied to each satellite for measurements of $y$ converging to a common trajectory, and the right plot shows the motion of the satellites in the $xy$ plane. The initial positions of the satellite are at the center, and the final positions are marked with an 'x.'

As in the previous case, our information flow approach greatly enhances stability. It is important to note that while the information flow law was restricted to those with good tracking performance at the reference trajectory frequencies, this is far less restrictive than the design of a controller

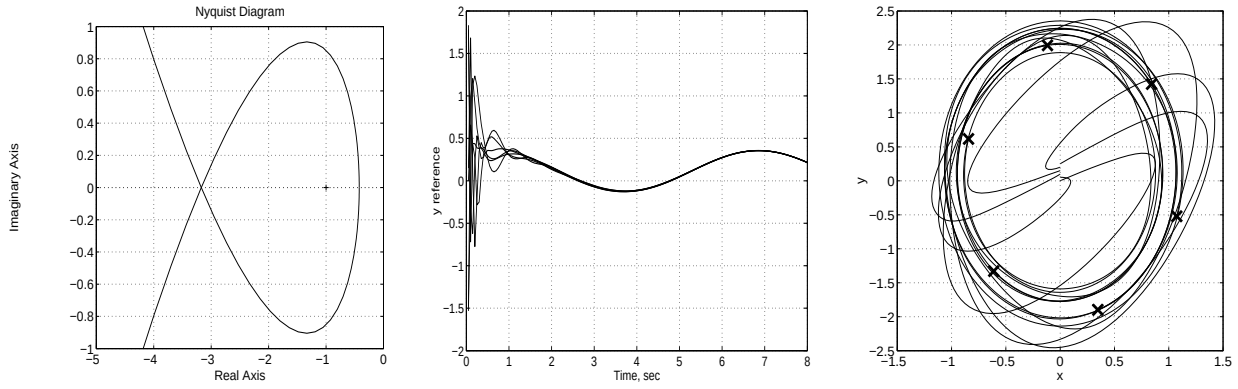


Figure 13: Satellite reconfiguration: nyquist plot for satellite information flow (left), convergence of satellite $y$-axis reference data (center), and satellite reconfiguration trajectories (right).

which stabilizes the vehicle dynamics. The difference is most noticeable in the presence of plant zeros, as would occur when only a subset of states are measurable.

# 6 Conclusions

The information flow law proposed in Section 5 shows the utility of the stability theorem in analyzing the behavior of vehicle formations and in synthesizing control solutions. We expect that this framework will be generally useful in analysis of formation stability problems and will be a useful starting point for future research. In particular, we expect that the qualitative insights into graph properties which are desirable from the perspective of stability can be quantified. A principle which allowed each vehicle in the graph to determine its impact on formation stability using only local information would be particularly useful, as it could form the basis of a protocol for information weighting.

In addition to separating information flow stability from vehicle stability, our approach to information flow can be shown to have good string stability properties, a subject which will be developed more fully in a future paper. Our approach relies on two key ideas. The first is the use of dynamical systems as a paradigm for understanding information exchange between vehicles, and the design of a dynamical system which enables the vehicles to achieve consensus on the formation center. The second is the use of feedforward compensation to render the sensed and transmitted information timely. While this paper restricts its focus to linear systems with fixed time delays, we expect that this approach can be extended to nonlinear vehicle systems and systems with variable time delays. Nonlinear systems typically possess a center manifold which corresponds to the surface on which the vehicle performs locomotion; if the information flow is restricted to that surface, it should be possible to extend the information flow principle to that class of problems. We

also conjecture that our approach can be extended to systems with variable time delays through appropriate extension of the feedforward term used to achieve stability separation.

At the moment, the main limitation in the method is the constraint that $c = 1$ in the information flow law. The need for consensus among vehicles forces the information flow law to be neutrally stable, which means that information never decays out. This renders the system sensitive to sensor errors and mismatches in initial conditions. One possibility for improvement is a protocol for resetting the information to zero periodically or in response to an event as a means of limiting any drift. Such a protocol could lie in a higher layer in the control architecture, and may itself require stability analysis. Alternate approaches to zeroing out accumulated error will be explored in the future.

## References

[1] J. G. Bender. An overview of systems studies of automated highway systems. *IEEE Transactions on Vehicular Technology*, 40(1):82–99, 1991.

[2] A. Berman and R. J. Plemmons. *Nonnegative Matrices in the Mathematical Sciences*. Academic Press, 1979.

[3] A. Berman and X.D. Zhang. Lower bounds for the eigenvalues of Laplacian matrices. *Linear Algebra and Applications*, 316(1-3):13–20, 2000.

[4] R. Burns et al. TechSat21: Formation design, control, and simulation. In *Proceedings of the IEEE Aerospace Conference*, pages 19–25, 2000.

[5] L. E. Buzogany, M. Pachter, and J. J. d'Azzo. Automated control of aircraft in formation flight. In *Proceedings of the AIAA Conference on Guidance, Navigation, and Control*, pages 1349–1370, 1993.

[6] F. R. K. Chung. *Spectral Graph Theory*, volume 92 of *Regional Conference Series in Mathematics*. American Mathematical Soc., 1997.

[7] W. H. Clohessy and R. S. Wiltshire. Terminal guidance system for satellite rendezvous. *Journal of the Aerospace Sciences*, 27(9):653–658, 1960.

[8] T. B. Curtin, J. G. Bellingham, J. Catipovic, and D. Webb. Autonomous oceanographic sampling networks. *Oceanography*, 6:86–94, 1993.

[9] D. Cvetkovic, M. Doob, and H. Sachs. *Spectra of Graphs*, volume 87 of *Pure and Applied Mathematics*. Academic Press, Inc., 1980.

[10] D. Cvetkovic, P. Rowlinson, and S. Simic. *Eigenspaces of Graphs*, volume 66 of *Encyclopedia of Mathematics and Applications*. Cambridge University Press, 1997.

[11] R. Diestel. *Graph Theory*, volume 173 of *Graduate Texts in Mathematics*. Springer-Verlag, 1997.

[12] M. Egerstedt, X. Hu, and A. Stotsky. Control of mobile platforms using a virtual vehicle approach. *IEEE Transactions on Automatic Control*, 46(11):1777–1782, 2001.

[13] J. A. Fax. *Optimal and Cooperative Control of Vehicle Formations*. Ph.D. thesis, California Institute of Technology, 2002.

[14] J. A. Fax and R. M. Murray. Graph laplacians and stabilization of vehicle formations. In *Proceeings of 15th IFAC Conference*, pages 283–288, 2002.

[15] J. A. Fax and R. M. Murray. Information flow and cooperative control of vehicle formations. In *Proceeings of 15th IFAC Conference*, pages 283–288, 2002.

[16] M. Fiedler. Algebraic connectivity of graphs. *Czechoslovak Mathematical Journal*, 23:298–305, 1973.

[17] S. Friedland and R. Nabben. On Cheeger-type inequalities for weighted graphs. Preprint.

[18] F. Giuletti, L. Pollini, and M. Innocenti. Autonomous formation flight. *IEEE Control Systems Magazine*, pages 34–44, December 2000.

[19] G. W. Hill. Researches in the lunar theory. *American Journal of Mathematics*, 1(1):5–26, 1878.

[20] R. Horn and C. Johnson. *Matrix Analysis*. Cambridge University Press, 1985.

[21] E. M. C. Kong. Optimal trajectories and optimal design for separated spacecraft interferometry. Master's thesis, Massachusetts Institute of Technology, 1999.

[22] N. E. Leonard and E. Fiorelli. Virtual leaders, artificial potentials and coordinated control of groups. In *Proceedings of the 40th IEEE Conference on Decision and Control*, pages 2968–2973, 2001.

[23] R. Merris. Laplacian matrices of graphs: A survey. *Linear Algebra and its Applications*, 197,198:143–176, 1994.

[24] R. Merris. A survey of graph Laplacians. *Linear and Multilinear Algebra*, 39:19–31, 1995.

[25] R. Nabben. Improved upper bounds for the real part of nonmaximal eigenvalues of nonnegative matrices. *SIAM Journal of Matrix Analysis and Applications*, 22(2):574–579, 2000.

[26] L. M. Pecora and T. L. Carroll. Master stability functions for synchronized coupled systems. *Physics Review Letters*, 80(10):2109–2112, 1998.

[27] H. Schaub et al. Spacecraft formation flying control using mean orbital elements. *Journal of the Astronautical Sciences*, 48(1):69–87, 2000.

[28] S. E. Shladover et al. Automatic vehicle control developments in the PATH program. *IEEE Transactions on Vehicular Technology*, 40(1):114–130, 1991.

[29] T. R. Smith, H. Hanßmann, and N. E. Leonard. Orientation control of multiple underwater vehicles. In *Proceedings of the 40th IEEE Conference on Decision and Control*, pages 4598–4603, 2001.

[30] D. Swaroop and J. K. Hedrick. Constant spacing strategies for platooning in automated highway systems. *ASME Journal of Dynamic Systems, Measurement and Control*, 121:462–470, 1999.

[31] R. S. Varga. *Matrix Iterative Analysis*, volume 27 of *Springer Series in Computational Mathematics*. Springer-Verlag, 2 edition, 1991.

[32] J. D. Wolfe, D. F. Chichka, and J. L. Speyer. Decetntralized controllers for unmanned aerial vehicle formation flight. In *Proceedings of AIAA Conference on Guidance, Navigation, and Control*, 1996. AIAA Paper 96-3833.

[33] D. Yanakiev and I. Kanellakopoulos. A simplified framework for string stability analysis in AHS. In *Proceedings of 13th IFAC World Congress*, volume Q, pages 177–182, San Francisco, CA, 1996.

[34] H.-H. Yeh, E. Nelson, and A. Sparks. Nonlinear tracking control for satellite formations. In *Proceedings of the 39th IEEE Conference on Decision and Control*, pages 328–333, 2000.

[35] K. Zhou and J. C. Doyle. *Essentials of Robust Control*. Prentice Hall, New Jersey, 1998.